Theoretical Study of the Structural and Electronic Properties of Si_mGe_n and $Si_mGe_n^-$ ($s = m + n \leq 7$) Clusters

Dan Bing, Quoc Chinh Nguyen, Xiao-feng Fan, and Jer-Lai Kuo*

School of Physical and Mathematical Sciences, Nanyang Technological University, Singapore 637371, Singapore

Received: November 26, 2007; In Final Form: December 24, 2007

Ground-state structures, vibrational frequencies, HOMO−LUMO energy gap, electron affinities, and cluster mixing energy of binary semiconductor clusters Si_mGe_n in the range $s = m + n \leq 7$ have been investigated using the B3LYP-DFT and CCSD(T) methods with the basis of 6-311+G(d). Si_mGe_n clusters are found to have similar structural patterns and the same spin multiplicities as those of corresponding elemental clusters of Si_s and Ge_s but with more isomeric structures and lower symmetries. Notable structural changes induced by the additional electron were observed, except for $s = 4$. The mixing energies of binary clusters are negative, which suggests that the mixed clusters are more stable than pure Si and Ge clusters. Both the HOMO−LUMO gaps and the calculated mixing energy show that binary clusters $SiGe_2$, Si_2Ge_2, Si_2Ge_3, Si_2Ge_4, and Si_2Ge_5 are species with high stability and more likely to be produced experimentally.

I. Introduction

Recently, there has been a growing interest in materials containing the group IV atoms C, Si, Ge, and Sn.[1−5] These materials are important due to their applications in the semiconductor and optoelectronic industries.[6−9] In addition to the pure elemental materials, many applications involve more than one type of element, whether in compounds, impurities, alloys, or interfaces. For example, Si−Ge materials have been studied extensively in the past years, and the binary heterostructure $Si/Si_{1-x}Ge_x$ has produced a new generation of high-performance heterojunction bipolar transistors (HBT), field effect transistors, and infrared detectors.[1,10]

Atomic-scale analysis on Si−Ge materials is becoming more and more important as semiconductor devices are constantly being scaled down. It is found that concepts obtained from SiGe in the bulk form may not be directly applicable to SiGe at the nanoscopic level due to enormous surface energy effects and lattice strains. Therefore, fundamental understanding of the structure and thermodynamic/electronic properties of Si−Ge nanoclusters would soon play an important role in the advancement in the nanoscale devices, especially in the interfacial areas where the lattice mismatch occurs due to the change of atomic composition. Furthermore, in most semiconductor and surface growth processes, chemical vapor deposition (CVD) methods are commonly used, and understanding of chemical and physical properties of such building block molecules is crucial in the production of the desired properties.[11−13]

For theoreticians, the elusive structures of these silicon and germanium molecules make them attractive systems for high-level ab initio treatment. The search for the global minima as well as their growth patterns for silicon clusters Si_s and germanium clusters Ge_s has received much theoretical attention.[5,14−21] Previous studies have confirmed that the global minimum silicon cluster Si_s and germanium clusters Ge_s have identical geometries up to $s = 12$.[17,22] The main difference is the increase in bond lengths of Ge clusters by about 4−5% compared to Si. Since the pure elemental clusters in this size range have identical geometries, it is reasonable to ask whether binary clusters Si_mGe_n would preserve such trend.

Up to now, mixed Si_mGe_n clusters remain underexplored compared to their elemental counterparts. Li and Jin[23] investigated the low-energy structures of Si_mGe_n (for $m + n \leq 10$) clusters using tight-binding methods based on averaged parameters of Si and Ge without frequency analysis. Later on, they performed a more extensive study on binary A_mB_n (A, B = Si, Ge, C and $m + n \leq 10$) clusters using the B3LYP-DFT method, but only on selected initial geometries with high symmetries.[24] They suggest that $SiGe_2$ has a triplet ground state, different from both Si_3 and Ge_3 which have singlet ground states. The possibility for an abrupt change of electronic properties by changing the stoichiometry motivates us to carry out a detailed and systematic study on all possible alloy combinations. Furthermore, calculations on anionic clusters, which are more relevant to experimental conditions, are also performed.

II. Computational Details

In this work, the B3LYP-DFT method with 6-311+*G*(*d*) basis set has been employed to optimize the geometries of neutral and anion semiconductor binary systems. Frequency analyses are also performed at the same theoretical level to check whether the optimized structures are transition states or true minima on the potential energy surfaces of corresponding cluster systems. With the use of the B3LYP optimized geometries, the energies of the clusters are calculated with coupled cluster singles and doubles including a perturbative estimate of triple excitations (CCSD(T)) method with the 6-311+*G*(*d*) basis set. The choice of B3LYP geometries in computing CCSD(T) energies has been verified for pure Ge cluster systems to get more satisfactory energy values at relatively lower computational cost.[25] All ab initio calculations reported in this work were performed with the Gaussian 03 package.[26]

The initial input structures of Si_mGe_n for the first principle investigations are constructed using the published structure of

* To whom correspondence should be addressed. E-mail: jlkuo@ntu.edu.sg.

10.1021/jp711172n CCC: $40.75
Published on Web 02/15/2008

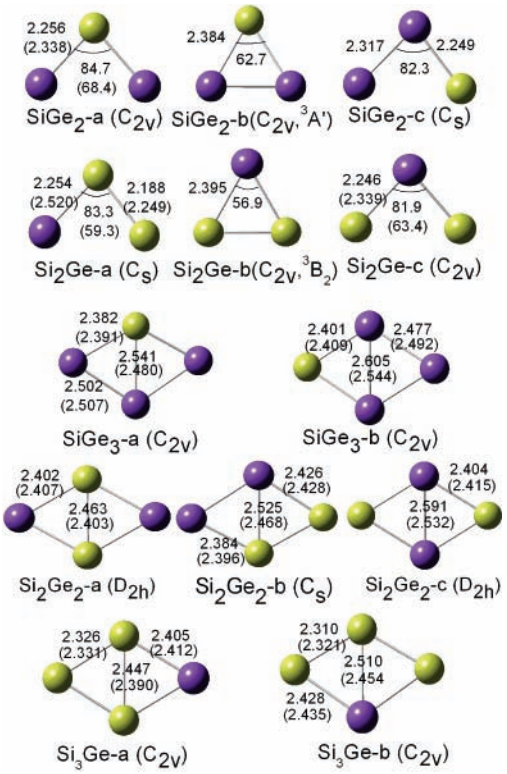

Figure 1. All of the equilibrium structures of the neutral and anion Si_mGe_n ($s = m + n = 3, 4$) clusters optimized at the B3LYP/6-311+G(*d*) level. (The bond lengths and angles of the anions are presented in parentheses.) Isomers are arranged according to their relative stability with the most stable structure on the right. One of the common trends in both neutral and anionic clusters is that the Si atom prefers to occupy the high-coordination position.

Si_s or Ge_s as templates.[15,25,27] To speed up our calculations, for $m > n$ we built the initial structures by replacing the n Si atoms by n Ge atoms from the Si_{m+n} template and for $m < n$ we replaced the Ge atoms by Si from the Ge_{m+n} template. Although all 2^{m+n} combinations within a given (m, n) can be generated straightforwardly, we have further used the symmetry of the template structure to reduce amount of calculations. Since all symmetrically related structures would have identical physical/chemical properties, only one representative is needed. This approach is useful especially for the highly symmetrical bipyramid templates (for $m + n = 5$, 6, and 7). It was suggested that in the small Si_s or Ge_s, triplet states can be more stable than the singlet state. Hence, we have optimized all the neutral clusters in both the singlet and triplet potential energy surfaces and optimized all anionic clusters on both doublet and quadruplet potential energy surfaces.

III. Results and Discussion

III.A. Equilibrium Structures of Si_mGe_n and $Si_mGe_n^-$. The ground-state geometries of the neutral and anion Si_mGe_n clusters are compared in Figures 1 and 2. Tables 1−III tabulate the calculated HOMO−LUMO gap and vibrational frequencies of the lowest energy structures obtained at the same theoretical level (B3LYP/6-311+$G(d)$) as that used in the optimization processes. Figure 3 shows the comparison of the bond length of neutral and anion clusters. Figure 4 shows the molecular orbitals to explain the structural changes by adding one electron to neutral ones. Throughout the work, cutoff distances are used to define whether a bond is formed between two atoms. The cutoff distance is determined by the bond length distribution of pure Si_s and Ge_s clusters. For $m + n \leq 5$, the cutoff of Si−Si and Ge−Ge is 2.7 and 2.8 Å, respectively. For $m + n \geq 6$, the cutoff of Si−Si and Ge−Ge is 3.3 and 3.5 Å, respectively. The cutoff of Si−Ge bond is taken as the average of those of Si−Si and Ge−Ge bonds.

III.A.1. Linear Si_mGe_n and $Si_mGe_n^-$ ($s = m + n = 2$). The ab initio results indicate that the total energy of the triplet SiGe cluster is 0.68 eV lower than that of the singlet cluster. This indicates that SiGe binary clusters have the same multiplicity as that of elemental dimers Si_2 and Ge_2 which have been confirmed in both experiments and theory.[25]

The bond distance, harmonic vibrational frequencies, dissociation energy, and dipole moment for the ground state of SiGe are listed in Table 1. Some calculated and experimental values in the literature are also listed for comparison.[2−4,11,24,28] For the SiGe diatomic molecule, Li et al.[4] measured an infrared spectrum in 1994. They obtained the SiGe sample by arc-melting the mixed metal under an argon atmosphere. They determined the fundamental vibrational frequency for the SiGe to be 419 cm^{-1} for the ground state. Our calculated frequency is 426 cm^{-1}, as shown in Table 1, in good agreement with the experimental value.

The predicted dipole moment for SiGe is very small, 0.19 D. The small dipole moment is mainly due to the fact that the standard electronegativity of silicon is 1.8, which is nearly equal to that of germanium. The result of Sari et al.[28] is 0.20 D, which agrees well with our calculation. From the satisfactory results of SiGe, the B3LYP/6-311+G(d) method is adequate to provide reliable properties of Si_mGe_n clusters.

III.A.2. Planar Structures of Triangular Si_mGe_n and $Si_mGe_n^-$ ($s = m + n = 3$). For Si_mGe_n ($s = m + n = 3$) binary clusters, linear structures are excluded in our discussion here due to the fact that they have extremely low stabilities in the pure clusters.[25,29] The theoretically optimized ground states are in singlet state with triangular shapes. As shown in Figure 1, $SiGe_2$ has three possible configurations. $SiGe_2$-a (C_{2v}) is more stable than $SiGe_2$-c (C_s) because of the bond energy order Si−Si > Si−Ge ($SiGe_2$-a has two Si−Ge bonds, whereas $SiGe_2$-c has one Si−Ge bond and one Ge−Ge bond). The simple estimate yields correct energetics other with the ab initio results. The energy of the triplet triangular $SiGe_2$-b is between that of $SiGe_2$-a and $SiGe_2$-c. Similarly, for Si_2Ge, the structure with Ge atom at the terminal of the bent linear structure has lower energy than the one with Ge in the middle. This is different from the results of Li et al.,[24] where they missed the C_s structure $SiGe_2$-a and took the triplet as the ground state. From this example, we can see that it is not guaranteed to find the ground state by considering only the highly symmetric structures.

When adding one electron to the neutral cluster, the bond angle becomes smaller and the bond length becomes longer. For example, $SiGe_2$ changes from 84.7° to 68.4° and from 2.256 to 2.338 Å. Thus, the additional of one electron to the cluster squeezes the open triangle into a closed one (the Ge−Ge bond in $SiGe_2$ changes from 3.040 to 2.629 Å).

III.A.3. Rhombus Si_mGe_n and $Si_mGe_n^-$ ($s = m + n = 4$). From the geometrical point of view, four-atom clusters are important as it can show the onset of three-dimensional (3D) evolution. Similar to Si_4 and Ge_4, planner rhombus are much more stable than both linear and tetrahedron structures, and the singlet state is much more stable than the triplet state. $SiGe_3$ has two isomers, one with the Si atom at short diagonal position, and another with the Si at long diagonal position. The calculated total electronic energy shows that silicon atoms prefer to occupy the short diagonal positions to form more stronger (Si−Si) bonds.

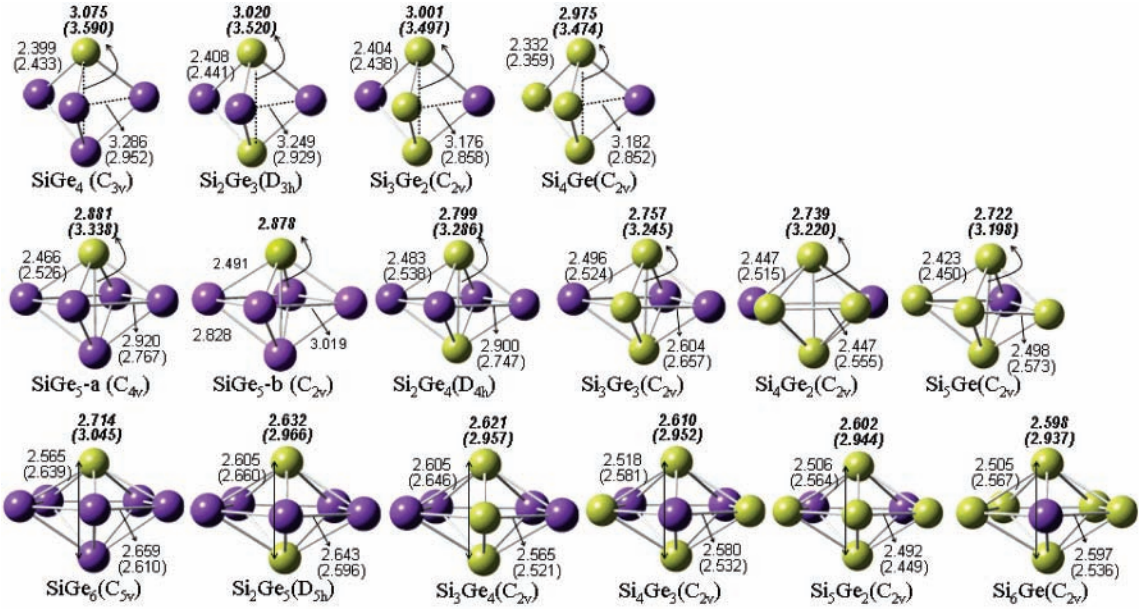

Figure 2. Lowest energy structures of all calculated minima of the bipyramid Si_mGe_n ($s = m + n = 5, 6, 7$) clusters optimized at the B3LYP/6-311+G(*d*) level. (The bond lengths of the anions are presented in parentheses.) The structures of other isomers can be found in the Supporting Information. The bond lengths between two apex atoms are given in bold italic font on the top; the bond lengths between the apex and base atoms are given on the top left; the bond lengths between base atoms are given on the bottom right. A common feature of structural changes upon adding one electron to the neutral clusters is the mutual repulsion of the two apex atoms in the vertical direction, while the planar atoms contract inward.

TABLE 1: Bond Distances (in angstroms), Harmonic Vibrational Frequencies (in cm^{-1}), Dissociation Energies (D_0, in eV), and Dipole Moments for the Ground State of SiGe at the B3LYP/6-311+G(d) Level

level of theory	*R*	ω	D_0	μ
B3LYP/6-311+G(d)	2.229	426	2.74	0.19
cc-pVQZ CCSD(T)[a]	2.315	411	3.01	0.20
B3LYP/6-311G(3df)[b]	2.22	431	2.9	
MRCI[c]	2.360	387		
LSD[d]	2.339	397	3.79	
experiment[e]		419		
experiment[f]			3.08 ± 0.22	

[a] Ref 28. [b] Ref 24. [c] Ref 11. [d] Ref 3. [e] Ref 4. [f] Ref 2.

Upon charging them negatively, the rhombus structures relax along the long diagonal direction, while the short diagonal atoms contract inward. However, the atomic relaxations associated with charging are very small, with interatomic distances changing by not more than a few percent. This indicates the rhombus structures are very stable, and a detailed discussion will be given in section B.

III.A.4. Bipyramid or Distorted Bipyramid Si_mGe_n and $Si_mGe_n^-$ ($s = m + n = 5, 6, 7$). As the cluster size increases, it becomes much more costly to locate the lowest energy structure by theoretical means because the number of possible geometries increases exponentially. For Si_mGe_n clusters with $s = m + n > 5$, there exist a great number of possible isomers with very little difference in structures and energies. For simplicity, only the most stable structures are given in Figure 2, and the others are given in the Supporting Information.

When $s = m + n = 5$, the Si_mGe_n cluster has a larger bond length between the base atoms than that of $s = 6$ and 7. For example, in Si_2Ge_3 it is 3.249 Å, whereas the Ge−Ge bond in Si_2Ge_5 is 2.643 Å. The $Si_mGe_n^-$ clusters, although retaining the triangle bipyramid motif, shrink the base triangle (from 3.249 to 2.929 Å in Si_2Ge_3) and increase the bond lengths between the two apex Si atoms (from 3.020 to 3.520 Å in Si_2Ge_3). This large relaxation from neutral to anion cluster will be discussed in the next section.

Pure Si_6 or Ge_6 clusters have an edge-caped trigonal bipyramid (C_{2v}) ground-state structure, and a square bipyramid (D_{4h}) local minimum structure which has very close energy to the ground state. Therefore, we take both of the two structures as the initial structures of the $m + n = 6$ mixed clusters. However, most of the edge-caped trigonal bipyramids are optimized to square bipyramids during the optimization process except for $SiGe_5$, which keeps the two different topologies. The square bipyramid $SiGe_5$-a (C_{4v}) is found to have one doubly degenerate imaginary frequency at $9i$ cm^{-1} (*e*). However, the value of the imaginary frequency is very small (which can be neglected) and the total electronic energy is the lowest of all the isomers. Edge-caped trigonal bipyramid $SiGe_5$-b (C_{2v}) is found to be a local minimum but has a higher energy than $SiGe_5$-a (C_{4v}). Therefore, we believe $SiGe_5$-a (C_{4v}) is the most stable structure. For $Si_mGe_n^-$, the changes upon charging the neutral clusters are similar to that of $s = 5$, with the two apex distances lengthened (from 2.799 to 3.286 Å in Si_2Ge_4) and the base atoms shrinking (from 2.900 to 2.749 Å in Si_2Ge_4).

The ground-state structure of the Si_7 or Ge_7 is a pentagonal bipyramid (D_{5h}). The binary clusters retain this structure but with lower symmetry according to different combination of *m* and *n*. Again, the Si atom prefers to occupy the apex position. The ground state of Si_4Ge_3 has two Si atoms on apex positions, and another two on the separate base positions, while another isomer with Si atoms occupying two nearby base positions has only a little higher energy than the ground state. The same trend is valid for Si_5Ge_2. This indicates that the arrangement of Si atoms between the base position does not affect the stability very much because the low coordination. In the case of the anion, the distance between two apex atoms is increased (from 2.632 to 2.966 Å in Si_2Ge_5), which shrinks the base pentagon by reducing the atom distance (from 2.643 to 2.596 Å in Si_2Ge_4). The changes of structures are similar to that of $s = 5$ and 6, but much smaller.

III.A.5. Structural Relaxations upon Charging Si_mGe_n Clusters Negatively. Atomic relaxations upon adding one electron to neutral are important in interpreting photoemission data on

TABLE 2: Calculated Electronic State, Electronic Energies E_t (hartree/Particle), Relative Energy E_{rel} (eV), HOMO−LUMO Energy Gaps E_{gap} (eV), and Harmonic Vibrational Frequencies (cm^{-1}) of Si_mGe_n Binary Clusters ($s = m + n = 2, 3, 4$)[a]

Si_mGe_n		electronic state	E_t	E_{rel}	E_{gap}	vibrational frequency
SiGe	a	$^3\Sigma$	**−2364.339745**	**0.00**		**426(σ)**
	b	$^1\Sigma$	−2364.314660	0.68	0.64	474(σ)
$SiGe_2$	a	**$^1A_1$**	**−4439.810177**	**0.00**	**2.45**	**110(a_1) 421(b_2) 423(a_1)**
	b	$^3A'$	−4439.800686	0.26	3.55	198(a_1) 210(b_2) 366(a_1)
	c	$^1A_1$	−4439.798616	0.31	2.29	123(a') 301(a') 425(a')
Si_2Ge	**a**	**$^1A'$**	**−2653.388387**	**0.00**	**2.41**	**144(a') 422(a') 536(a')**
	b	$^3B_2$	−2653.382889	0.15	3.59	237(a') 237(a') 435(a')
	c	$^1A_1$	−2653.376600	0.32	2.31	138(a_1) 421(a_1) 432(b_2)
$SiGe_3$	**a**	**$^1A_1$**	**−6515.278697**	**0.00**	**2.41**	**66(b_1) 140(a_1) 203(a_1) 240(b_2) 340(a_1) 397(b_2)**
	b	$^1A_1$	−6515.273970	0.13	2.30	68(b_1) 144(b_2) 210(a_1) 265(a_1) 271(b_2) 381(a_1)
Si_2Ge_2	**a**	**^1A_g**	**−4728.863544**	**0.00**	**2.49**	**75(b_{3u}) 177(b_{2u}) 212(a_g) 366(b_{3g}) 391(b_{1u}) 403(a_g)**
	b	$^1A'$	−4728.860586	0.08	2.36	79(a'') 161(a') 237(a') 298(a') 358(a') 462(a')
	c	^1A_g	−4728.856574	0.19	2.29	80(b_{3u}) 179(b_{2u}) 231(a_g) 294(b_{3g}) 377(a_g) 384(b_{1u})
Si_3Ge	**a**	**$^1A_1$**	**−2942.444545**	**0.00**	**2.42**	**87(b_1) 200(b_2) 268(a_1) 398(b_2) 408(a_1) 473(a_1)**
	b	$^1A_1$	−2942.442341	0.06	2.35	91(b_1) 194(a_1) 301(a_1) 315(b_2) 416(a_1) 484(b_2)

[a] E_t and E_{rel} at the CCSD(T)/B3LYP/6-311+G(d) level, the others at the B3LYP/6-311+G(d) level.

TABLE 3: Calculated Electronic State, HOMO−LUMO Energy Gaps E_{gap} (eV), and Harmonic Vibrational Frequencies (cm^{-1}) of the Lowest Energy Si_mGe_n Binary Clusters ($s = m + n = 5, 6, 7$) at the B3LYP/6-311+G(d) Level

Si_mGe_n		E_{gap}	vibrational frequency
$SiGe_4$	$^1A_1$	3.14	107(e) 107(e) 144(a_1) 199(e) 199(e) 225(e) 317(e) 317(e) 354(a_1)
Si_2Ge_3	**$^1A_1'$**	**3.23**	118(e') 118(e') 155(a_1') 266(e'') 266(e'') 307(a_2'') 333(e') 333(e') 384(a_1')
Si_3Ge_2	$^1A_1$	3.07	122(a_1) 155(b_2) 180(a_1) 272(a_2) 287(b_1) 337(b_2) 356(b_1) 368(a_1) 439(a_1)
Si_4Ge	$^1A_1$	3.07	147(b_2) 165(a_1) 201(a_1) 282(b_1) 334(a_2) 357(a_1) 368(b_1) 429(b_2) 448(a_1)
$SiGe_5$-a	$^1A_1$	3.21	9i(e) 9i(e) 59(b_2) 143(b_1) 179(a_1) 200(a_1) 210(b_2) 221(e) 221(e) 331(a_1) 334(e) 334(e)
$SiGe_5$-b	$^1A'$	3.19	16(a'') 24(a') 59(a') 145(a'') 178(a') 200(a') 208(a') 220(a'') 221(a') 328(a') 331(a'') 337(a')
Si_2Ge_4	**$^1A_{1g}$**	**3.39**	22(e_u) 22(e_u) 52(b_{2u}) 148(b_{2g}) 200(a_{1g}) 213(b_{1g}) 245(a_{2u}) 316(e_g) 316(e_g) 328(e_u) 328(e_u) 372(a_{1g})
Si_3Ge_3	$^1A_1$	3.33	50(b_2) 60(a_1) 71(b_1) 208(a_1) 212(b_2) 249(b_1) 267(a_1) 304(a_2) 334(b_2) 342(b_1) 377(a_1) 400(a_1)
Si_4Ge_2	$^1A_1$	3.34	23(b_2) 61(a_1) 84(a_2) 233(a_1) 254(b_1) 268(a_1) 281(b_2) 339(a_2) 341(b_1) 381(a_1) 394(b_2) 430(a_1)
Si_5Ge	$^1A_1$	3.19	38(b_2) 97(a_1) 103(b_1) 262(b_2) 272(a_1) 274(b_1) 343(a_2) 344(a_1) 362(b_1) 399(a_1) 429(b_1) 433(a_1)
$SiGe_6$	$^1A_1$	3.03	84(e_2) 84(e_2) 127(e_1) 127(e_1) 136(a_1) 156(e_2) 156(e_2) 190(e_1) 190(e_1) 191(e_2) 191(e_2) 208(a_1) 308(e_1) 308(e_1) 313(a_1)
Si_2Ge_5	**$^1A_1'$**	**3.13**	80(e_2'') 80(e_2'') 149(e_1') 149(e_1') 160(e_2') 160(e_2') 169(a_2'') 194(e_2') 194(e_2') 215(a_1') 270(e_1'') 270(e_1'') 296(e_1') 296(e_1') 370(a_1')
Si_3Ge_4	$^1A_1$	3.01	83(a_2) 105(a_1) 149(b_2) 152(a_1) 165(a_1) 178(b_1) 182(b_2) 204(a_1) 249(b_2) 253(a_1) 274(a_2) 287(b_1) 304(b_2) 351(a_1) 383(a_1)
Si_4Ge_3	$^1A_1$	3.07	102(a_2) 113(b_1) 150(a_1) 154(b_2) 190(b_1) 201(a_1) 209(b_2) 238(a_1) 252(b_2) 280(b_1) 298(a_2) 298(a_1) 336(a_1) 369(b_2) 389(a_1)
Si_5Ge_2	$^1A_1$	3.05	114(b_1) 132(a_2) 159(a_1) 186(b_2) 199(b_1) 209(a_1) 230(b_2) 268(b_2) 274(a_1) 289(a_2) 307(b_1) 336(a_1) 356(b_2) 381(a_1) 402(a_1)
Si_6Ge	$^1A_1$	3.05	127(b_1) 154(a_2) 176(b_2) 205(a_1) 208(b_1) 233(a_1) 252(b_2) 287(a_1) 305(b_1) 314(a_2) 324(b_2) 343(a_1) 378(a_1) 394(b_2) 412(a_1)

negatively charged clusters.[30] Although the overall morphology of the anionic clusters remained similar to that of their neutral counterparts, notable structural changes occur depending on the size of the cluster due to the charge polarization induced by the additional electron. Figure 3 shows the comparison of the bond length of neutral and anion clusters. Points above (below) the diagonal line are the bonds lengthened (shortened) upon adding an electron to the neutrals. From Figure 3 we can see clearly the size dependence of the structural relaxation. Except for $s = 4$, atomic relaxations as a result of charging are substantial with changes in the interatomic distances and bond angles typically up to about 18%.

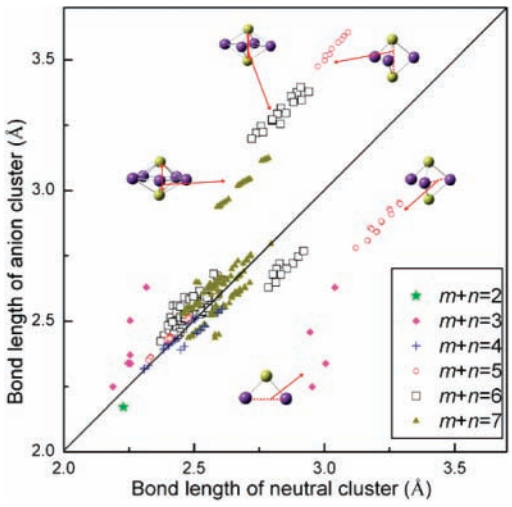

Figure 3. Comparison of bond lengths of all the low-energy Si_mGe_n vs $Si_mGe_n^-$ clusters in the structures optimized at the B3LYP/6-311+G(d) level. Each point represents a bond length of a cluster. Points above (below) the diagonal line are the bonds lengthened (shortened) upon adding an electron to the neutrals.

When $s = m + n = 5, 6, 7$, the binary clusters have bipyramid or distorted bipyramid structures. Silicon atoms prefer to occupy the apex positions, and the Ge atom prefers to occupy the lower coordination (base atom) over the apex position, indicating

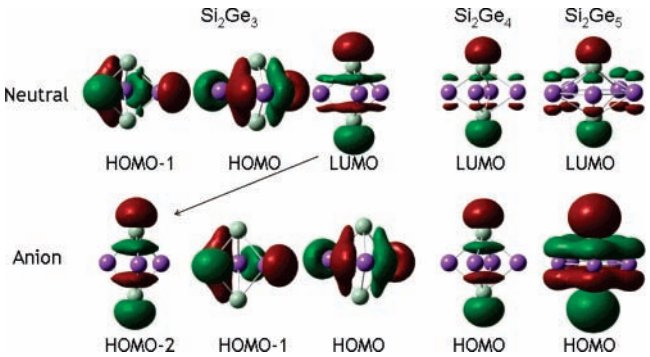

Figure 4. Molecular orbitals of Si_2Ge_3, Si_2Ge_4, and Si_2Ge_5 at the B3LYP/6-311+G(d) level. The antibonding orbital of the two apex atoms makes the bond lengthen upon adding one electron to the neutral. However, for $s = 5$, the HOMO of the anion and LUMO of the neutral are different and the LUMO of neutral cluster corresponds to the LUMO−2 in the anion. This reordering of the orbitals is related to the substantial relaxation in $s = 5$.

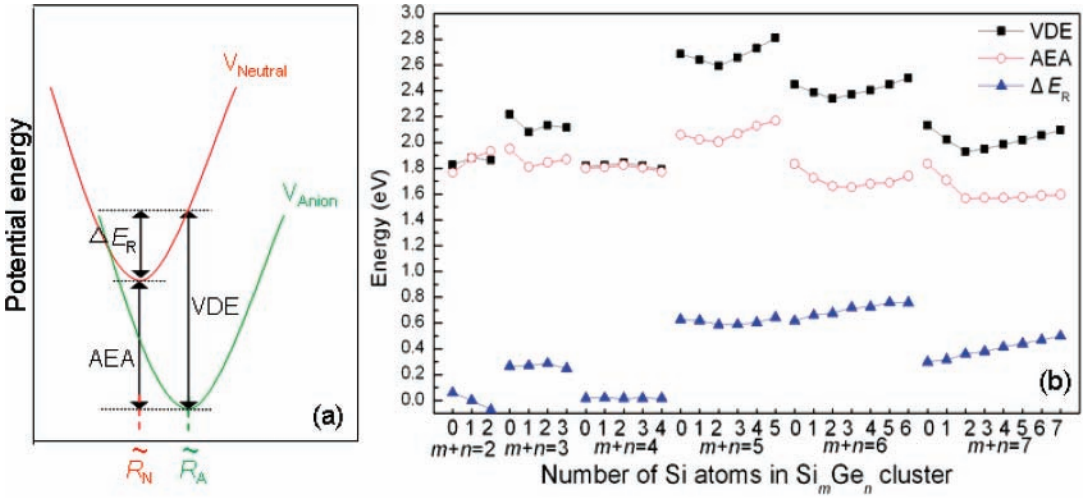

Figure 5. (a) Schematic representation of the definition of adiabatic electron attachment (AEA) energy, vertical detachment energy (VDE), and relaxation energy (ΔE_R). (b) AEA, VDE, and (ΔE_R) of the $Si_mGe_n^-$ cluster calculated at the CCSD(T)//B3LYP/6-311+G(d) level. ΔE_R = VDE − AEA.

directional bonding between Si−Ge bonds. A common feature of the relaxations as a result of charging is the mutual repulsion of the two apex atoms in the vertical direction, while the planar atoms contract inward. This is because the LUMO in the neutral case has antibonding character centered on the apex atoms, as shown in Figure 4. Usually, when adding one electron to the neutral cluster, the electron will occupy the LUMO orbital. Under the Koopman's theorem, the LUMO of the anion and HOMO of neutral molecules would be the same, and this is indeed the case for $s = 6, 7$. However, for $s = 5$, the HOMO of the anion and LUMO of the neutral are different and the LUMO of the neutral cluster corresponds to the LUMO−2 in the anion. This reordering of the orbitals is related to the substantial relaxation in $s = 5$.

III.B. Electron Affinities. Electron affinities of a cluster are important parameters in understanding its chemical stability. Calculated electron affinities, when compared with experimental data, help to distinguish between various low-energy isomers.[30] A schematic drawing to illustrate the definition of vertical electron detachment energies (VDE) of the anions, adiabatic electron affinities (AEA) of the neutral clusters, and relaxation energies (ΔE_R) is presented in Figure 5a. The AEA is equal to the difference between the total energies of a neutral system and the corresponding anion. The VDE correspond to transitions from the ground electronic state of the anion to the identical geometry in the neutral molecule ground electronic state, so the VDE should be higher than AEA. The ΔE_R is calculated by the difference between VDE and AEA. Therefore, ΔE_R indicates the geometrical changes between the neutral and anion clusters. The AEA, VDE, and ΔE_R are calculated as[31]

$$\text{AEA} = E(\text{optimized neutral}) - E(\text{optimized anion}) \quad (1)$$

$$\text{VDE} = E(\text{neutral at optimized anion geometry}) - E(\text{optimized anion}) \quad (2)$$

$$\Delta E_R = \text{VDE} - \text{AEA} \quad (3)$$

The computed VDE, AEA, and ΔE_R of Si_mGe_n clusters are presented in Figure 5b. From Figure 5b we can see that Si_mGe_n clusters with $s = m + n = 4$ and 7 have lower AEA and ΔE_R than their neighboring clusters, indicating that they are magic number clusters which are geometrically and electronically stable. These are agreed with the fact that the pure Si_4, Si_7 and Ge_4, Ge_7 clusters are also magic number clusters.[15,32,33] Especially for the cluster size 4, there is a very small difference of about 0.02 eV between the calculated VDE and EA, consistent with very little geometrical relaxation accompanying achment of an electron from the ground state of the neutral cluster. The larger relaxation energy for cluster sizes 5 and 6 indicates a significant structural transition upon addition of an electron on it. For structures which undergo significant atomic relaxations upon charging, a considerable portion of the electron affinity is associated with these relaxations.

VDE, AEA, and HOMO−LUMO gap can be measured experimentally using the anion photoelectron spectrometer. In the anion photoelectron spectra, the positions of the intensity maxima of the lowest energy bands determined the VDE. The onset energy of band yields the AEA. The first gap in the photoelectron spectrum corresponds to the HOMO−LUMO gap in the neutral clusters. However, in some cases, the exact onset is unclear because the band tails off slowly toward high electron kinetic energy; these tails are attributed to vibrationally hot anions. Thus, accurate AEA and the HOMO−LUMO gap cannot be obtained from the photoelectron spectra data alone. To our knowledge, there are no such experiments for mixed Si_mGe_n cluster. The theoretical predictions in the present work serve as useful references for future photoionization threshold measurements and photoelectron spectroscopy studies of semiconductor binary clusters.

III.C. Mixing Energy. The mixing energy corresponds to the change in energy on constructing the alloy cluster from identical configurations of the elemental clusters. A negative value of ΔE_{mix} corresponds to a nanoalloy cluster which is thermodynamically stable with respect to pure elemental clusters of the same size. The mixing energy of the two components in a bulk alloy or a cluster can be used as a measure of stability.[34] The mixing energy of Si_mGe_n clusters per atom can be expressed as

$$\Delta E_{mix} = \left[E(Si_mGe_n) - \frac{m}{m+n}E(Si_mSi_n) - \frac{n}{m+n}E(Ge_mGe_n)\right]/(m+n) \quad (4)$$

where $E(Si_mGe_n)$ is the potential energy of the Si_mGe_n cluster and $E(Si_mSi_n)$ and $E(Ge_mGe_n)$ are the potential energies of the Si_mSi_n and Ge_mGe_n clusters which have the identical configu-

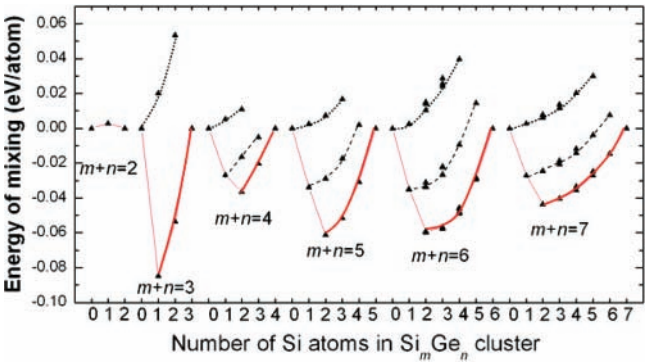

Figure 6. Mixing energy of all the Si_mGe_n clusters at the CCSD(T)//B3LYP/6-311+G(d) level (their structures are given in the Supporting Information). The red line highlights the lowest energy structures. The solid lines on the bottom correspond to the structures with both apex positions (high-coordination atom) occupied by two Si atoms, which are the most stable configurations. The dotted lines on the top correspond to the structures with both apex positions occupied by two Ge atoms, which are the most unstable configurations. The dashed lines in the middle correspond to the structures with one apex occupied with Si and another with Ge, whose stabilities are between the former two extremes.

ration of the binary cluster. The cluster energies of mixing ΔE_{mix} of different compositions are calculated according to eq 4.

The calculated results are shown in Figure 6. The cluster mixing energies ΔE_{mix} of Si_mGe_n are negative, which suggests that the mixed clusters are more stable than pure Si and Ge clusters, so they are possible to be produced experimentally. From $s = 4-7$, the mixing energy divided into three lines for each size (two lines for $s = 3$), which indicates the different levels of stability. The solid lines on the bottom correspond to the structures with both apex positions (low coordination atom) occupied by two Si atoms, which are the most stable configurations. The dotted lines on the top correspond to the structures with both apex positions occupied by two Ge atoms, which are the most unstable configurations. The dashed lines in the middle correspond to the structures with one apex occupied with Si and another with Ge, whose stabilities are between the former two extremes. Among the different configurations with the same composition, the most stable structure has the smallest mixing energy.

From Figure 6 we can see that $SiGe_2$, Si_2Ge_2, Si_2Ge_3, Si_2Ge_4, and Si_2Ge_5 have the lowest mixing energy of the same-sized clusters; therefore, they are the most stable clusters of each size. These stable clusters have structures where all Si atoms are in high-coordination positions, and Ge atoms are in low-coordination positions. These clusters are also found to have the highest HOMO−LUMO gaps of the same-sized clusters.

Apart from SiGe and the four-atom cluster, the mixing energy becomes larger as the cluster size increases. It has been confirmed that the mixing free energy of bulk SiGe alloy is positive at 0 K;[35] then there must exist a critical size at which the mixing energy becomes positive. It will be very interesting to find out at what size the transition will occur.

IV. Conclusions

In this work we have systematically studied the neutral and anionic Si_mGe_n ($s = m + n \leq 7$) clusters for all choices of m and n. The lowest energy isomers have been identified for all the combinations of m and n, as well as several of the lowest-lying isomers. We have examined all neutral clusters in both singlet and triplet potential energy surfaces and found that all the most stable neutral clusters are in singlet states except for the dimers. All the anionic clusters were optimized in both doublet and quadruplet states, and the stable structures in a given (m, n) are all in doublet states. In short, binary clusters are found to have similar ground-state structures and spin multiplicity as the corresponding elemental clusters. We should point out that the singlet state Si_2Ge-a (C_s) is found to be more stable than the triplet state (C_{2v}), which is different from Li et al.'s conclusion that Si_2Ge has a triplet ground state[24] based on studying selected isomers with high symmetry. This discrepancy shows that one should not be biased toward the highly symmetric structures and a detailed searching is necessary for identifying the global minima structures.

The overall morphology of anionic clusters remained similar to that of their neutral counterparts, but notable structural relaxations due to the charge polarization induced by the additional electron were observed. Except for $s = 4$, atomic relaxations as a result of charging are substantial with changes in the interatomic distances and/or bond angles typically up to about 18%. For $s = 5$, 6, and 7, a common feature of the relaxations is the mutual repulsion of the two apex atoms in the vertical direction, while the planar atoms contract inward. This is in line with that fact because the LUMO in the neutral case has antibonding character that is centered on the apex atoms.

The mixing energies of binary clusters are negative, which suggests that the mixed clusters are more stable than pure Si and Ge clusters (except for the triplet SiGe, which has small value positive mixing energy). It has been confirmed that the mixing free energy of bulk SiGe alloy is positive at 0 K, so it will be very interesting to find out at what size the transition of mixing energy from negative to positive will occur.

Our calculation also suggests that among the small-sized clusters, $SiGe_2$, Si_2Ge_2, Si_2Ge_3, Si_2Ge_4, and Si_2Ge_5 with large HOMO−LUMO gaps and most negative mixing energies should be prominent in growth experiments because of strong chemical stabilities. It would be very interesting to compare our predictions with the actual formation of clusters in a CVD growth environment for bulk Si−Ge solids or films. Results obtained in this work present a foundation for future theoretical and experimental study of group IV binary clusters.

Acknowledgment. This work was supported by Nanyang Technological University and Ministry of Education of Singapore under URC Grants (RG34/05 and RG57/05).

Supporting Information Available: Structures (in *xyz* format) of all neutral and anionic Si_mGe_n clusters considered in this work. This material is available free of charge via the Internet at http://pubs.acs.org.

References and Notes

(1) De Salvador, D.; Petrovich, M.; Berti, M.; Romanato, F.; Napolitani, E.; Drigo, A.; Stangl, J.; Zerlauth, S.; Muhlberger, M.; Schafffler, F.; Bauer, G.; Kelires, P. C. *Phys. Rev. B* **2000**, *61*, 13005.

(2) Drowart, J.; Maria, G. D.; Boerboom, A. J. H.; Inghram, M. G. *J. Chem. Phys.* **1959**, *30*, 308.

(3) Jan, A.; Nino, R.; Dennis, R. S. *J. Chem. Phys.* **1987**, *87*, 6562.

(4) Li, S.; Van Zee, R. J.; Weltner, W. *Chem. Phys. Lett.* **1994**, *229*, 531.

(5) Bai, J.; Cui, L. F.; Wang, J. L.; Yoo, S. H.; Li, X.; Jellinek, J.; Koehler, C.; Frauenheim, T.; Wang, L. S.; Zeng, X. C. *J. Phys. Chem. A* **2006**, *110*, 908.

(6) Shim, I.; Sai Baba, M.; Gingerich, K. A. *Chem. Phys.* **2002**, *277*, 9.

(7) Abbate, G.; Barone, V.; Lelj, F.; Iaconis, E.; Russo, N. *Surf. Sci.* **1985**, *152−153*, 690.

(8) Gazicki, M.; Szymanowski, H.; Tyczkowski, J.; Malinovsky, L.; Schalko, J.; Fallmann, W. *Thin Solid Films* **1995**, *256*, 31.

(9) Kumar, S.; Trodahl, H. J. *Thin Solid Films* **1990**, *193*−*194*, 72.
(10) Maiti, C. K.; Bera, L. K.; Maikap, S.; Ray, S. K.; Chakrabarti, N. B.; Kesavan, R.; Kumar, V. *Def. Sci. J.* **2000**, *50*, 299.
(11) Sefyani, F. L.; Schamps, J.; Delaval, J. M. *J. Mol. Spectrosc.* **1993**, *162*, 269.
(12) Schmude, R. W.; Gingerich, K. A.; Kingcade, J. E. *J. Phys. Chem.* **1995**, *99*, 15294.
(13) Shim, I.; Baba, M. S.; Gingerich, K. A. *J. Phys. Chem. A* **1998**, *102*, 10763.
(14) Ho, K.-M.; Shvartsburg, A. A.; Pan, B.; Lu, Z.-Y.; Wang, C.-Z.; Wacker, J. G.; Fye, J. L.; Jarrold, M. F. *Nature* **1998**, *392*, 582.
(15) Sandeep, N.; Chiranjib, M.; Kulshreshtha, S. K. *J. Chem. Phys.* **2006**, *125*, 074303.
(16) Waldemar, H.; Hennig, R. G.; Stefan, G.; Umrigar, C. J.; Bernard, D.; Lenosky, T. *Phys. Rev. B: Condens. Matter Mater. Phys.* **2007**, *75*, 085411.
(17) Shvartsburg, A. A.; Liu, B.; Lu, Z.-Y.; Wang, C.-Z.; Jarrold, M. F.; Ho, K.-M. *Phys. Rev. Lett.* **1999**, *83*, 2167.
(18) Yoo, S.; Zeng, X. C.; Zhu, X. L.; Bai, J. *J. Am. Chem. Soc.* **2003**, *125*, 13318.
(19) Zhao, J.; Wang, J.; Jellinek, J.; Yoo, S.; Zeng, X. C. *Eur. Phys. J. D* **2005**, *34*, 35.
(20) Yoo, S. H.; Zeng, X. C. *Angew. Chem., Int. Ed.* **2005**, *44*, 1491.
(21) Takahashi, M.; Kawazoe, Y. *Chem. Phys. Lett.* **2006**, *418*, 475.
(22) Cheshnovsky, O.; Yang, S. H.; Pettiette, C. L.; Craycraft, M. J.; Liu, Y.; Smalley, R. E. *Chem. Phys. Lett.* **1987**, *138*, 119.
(23) Li, S. D.; Jin, Z. H. *Chem. J. Chin. Univ. (in Chinese)* **2000**, *21*, 1468.
(24) Li, S.-D.; Zhao, Z.-G.; Zhao, X.-F.; Wu, H.-S.; Jin, Z.-H. *Phys. Rev. B* **2001**, *64*, 195312.
(25) Edet, F. A.; Alain, S.-A. *J. Chem. Phys.* **1998**, *109*, 962.
(26) Frisch, M. J.; Trucks, G. W.; Schlegel, H. B.; Scuseria, G. E.; Robb, M. A.; Cheeseman, J. R.; Montgomery, J. A., Jr.; Vreven, T.; Kudin, K. N.; Burant, J. C.; Millam, J. M.; Iyengar, S. S.; Tomasi, J.; Barone, V.; Mennucci, B.; Cossi, M.; Scalmani, G.; Rega, N.; Petersson, G. A.; Nakatsuji, H.; Hada, M.; Ehara, M.; Toyota, K.; Fukuda, R.; Hasegawa, J.; Ishida, M.; Nakajima, T.; Honda, Y.; Kitao, O.; Nakai, H.; Klene, M.; Li, X.; Knox, J. E.; Hratchian, H. P.; Cross, J. B.; Bakken, V.; Adamo, C.; Jaramillo, J.; Gomperts, R.; Stratmann, R. E.; Yazyev, O.; Austin, A. J.; Cammi, R.; Pomelli, C.; Ochterski, J. W.; Ayala, P. Y.; Morokuma, K.; Voth, G. A.; Salvador, P.; Dannenberg, J. J.; Zakrzewski, V. G.; Dapprich, S.; Daniels, A. D.; Strain, M. C.; Farkas, O.; Malick, D. K.; Rabuck, A. D.; Raghavachari, K.; Foresman, J. B.; Ortiz, J. V.; Cui, Q.; Baboul, A. G.; Clifford, S.; Cioslowski, J.; Stefanov, B. B.; Liu, G.; Liashenko, A.; Piskorz, P.; Komaromi, I.; Martin, R. L.; Fox, D. J.; Keith, T.; Al-Laham, M. A.; Peng, C. Y.; Nanayakkara, A.; Challacombe, M.; Gill, P. M. W.; Johnson, B.; Chen, W.; Wong, M. W.; Gonzalez, C.; Pople, J. A. *Gaussian 03*; Gaussian, Inc.: Wallingford, CT, 2004.
(27) Li, B.-X.; Cao, P.-L.; Song, B.; Ye, Z.-Z. *Phys. Lett. A* **2003**, *307*, 318.
(28) Levent, S.; Yukio, Y.; Henry, F. S., III. *J. Chem. Phys.* **2003**, *119*, 8266.
(29) Raghavachari, K. *J. Chem. Phys.* **1986**, *84*, 5672.
(30) Ogut, S.; Chelikowsky, J. R. *Phys. Rev. B* **1997**, *55*, R4914.
(31) Bouteiller, Y.; Desfrancois, C.; Scherman, J. P.; Latajka, Z.; Silvi, B. *J. Chem. Phys.* **1998**, *108*, 7967.
(32) Zhang, Q. L.; Liu, Y.; Curl, R. F.; Tittel, F. K.; Smalley, R. E. *J. Chem. Phys.* **1988**, *88*, 1670.
(33) Wang, J.; Zhao, J.; Ding, F.; Shen, W.; Lee, H.; Wang, G. *Solid State Commun.* **2001**, *117*, 593.
(34) Jellinek, J.; Krissinel, E. B. *Chem. Phys. Lett.* **1996**, *258*, 283.
(35) Qteish, A.; Resta, R. *Phys. Rev. B* **1988**, *37*, 6983.